

Clocking Femtosecond Collisional Dynamics via Resonant X-Ray Spectroscopy

Q. Y. van den Berg,^{1,*} E. V. Fernandez-Tello,² T. Burian,^{3,4} J. Chalupský,³ H.-K. Chung,⁵ O. Ciricosta,¹
 G. L. Dakovski,⁶ V. Hájková,³ P. Hollebon,¹ L. Juha,^{3,4} J. Krzywinski,⁶ R. W. Lee,⁷ M. P. Minitti,⁶
 T. R. Preston,¹ A. G. de la Varga,² V. Vozda,³ U. Zastra,⁸ J. S. Wark,¹
 P. Velarde,² and S. M. Vinko^{1,†}

¹*Department of Physics, Clarendon Laboratory, University of Oxford, Parks Road, Oxford OX1 3PU, United Kingdom*

²*Instituto de Fusión Nuclear, Universidad Politécnica de Madrid, José Gutiérrez Abascal 2, 28006 Madrid, Spain*

³*Institute of Physics ASCR, Na Slovance 2, 18221 Prague 8, Czech Republic*

⁴*Institute of Plasma Physics CAS, Za Slovankou 3, 182 00 Prague 8, Czech Republic*

⁵*Atomic and Molecular Data Unit, Nuclear Data Section, IAEA, P.O. Box 100, A-1400 Vienna, Austria*

⁶*SLAC National Accelerator Laboratory, 2575 Sand Hill Road, Menlo Park, California 94025, USA*

⁷*Department of Physics, University of California, Berkeley, California 94720, USA*

⁸*European XFEL, Holzkoppel 4, 22869 Schenefeld, Germany*



(Received 21 July 2017; revised manuscript received 6 November 2017; published 1 February 2018)

Electron-ion collisional dynamics is of fundamental importance in determining plasma transport properties, nonequilibrium plasma evolution, and electron damage in diffraction imaging applications using bright x-ray free-electron lasers (FELs). Here we describe the first experimental measurements of ultrafast electron impact collisional ionization dynamics using resonant core-hole spectroscopy in a solid-density magnesium plasma, created and diagnosed with the Linac Coherent Light Source x-ray FEL. By resonantly pumping the $1s \rightarrow 2p$ transition in highly charged ions within an optically thin plasma, we have measured how off-resonance charge states are populated via collisional processes on femtosecond time scales. We present a collisional cross section model that matches our results and demonstrates how the cross sections are enhanced by dense-plasma effects including continuum lowering. Nonlocal thermodynamic equilibrium collisional radiative simulations show excellent agreement with the experimental results and provide new insight on collisional ionization and three-body-recombination processes in the dense-plasma regime.

DOI: [10.1103/PhysRevLett.120.055002](https://doi.org/10.1103/PhysRevLett.120.055002)

Collisional interactions between electrons and ions play a fundamental role in describing the nonequilibrium behavior of plasmas in the warm- and hot-dense matter regimes. They directly influence the charge state distribution [1] and, hence, indirectly plasma transport properties [2–4], optical properties [5,6], and equilibration time scales [7]. A detailed understanding of collisional mechanisms is of great practical importance for research in inertial confinement fusion [8] and in astrophysical plasmas [9]. With the advent of bright x-ray free-electron laser light sources (XFELs) and diffract-before-destroy techniques [10], understanding the time scales of electron dynamics, and, in particular, collisional ionization, is also increasingly important given its role as a driver of electronic damage in biomolecular imaging experiments [11,12]. Nevertheless, measuring collisional ionization (CI) rates in dense plasmas poses many experimental challenges related to the extremely short time scale on which they take place and to the general difficulty of creating a well-characterized dense plasma at or near local thermodynamic equilibrium (LTE) [13]. XFELs now provide access to these extreme regimes: Recent experiments on the Linac Coherent Light Source (LCLS) [14] facility at SLAC have shown that

XFEL pulses are sufficiently intense to heat samples placed in the focus of the beam to temperatures approaching 200 eV within a few tens of femtoseconds [15–17].

The most common methods used to study collisional ionization rates in plasmas are based on crossed beam [18–20] and ion trap techniques [21–23]. Crossed beam experiments allow for a high energy resolution in collisional cross section measurements, but their use is restricted to lowly charged ionic charge states due to the cross section decreasing with the charge and the difficulty of producing sufficiently large ion beam currents [24]. In contrast, ion trap methods allow for measurements up to higher charge states, provided that the plasma conditions are well defined and that the atomic transition of interest can be isolated from other competing processes [25]. Both methods are, however, limited to electron number densities $\lesssim 10^{17} \text{ cm}^{-3}$ [26].

Here we present resonant core-hole spectroscopy measurements of collisional ionization rates in well-characterized, optically thin magnesium plasmas, created and diagnosed on femtosecond time scales with the LCLS XFEL. Our electron densities are that of highly ionized, solid-density Mg, in the range 10^{23} – 10^{24} cm^{-3} , well into the strong-coupling warm-dense matter regime. The

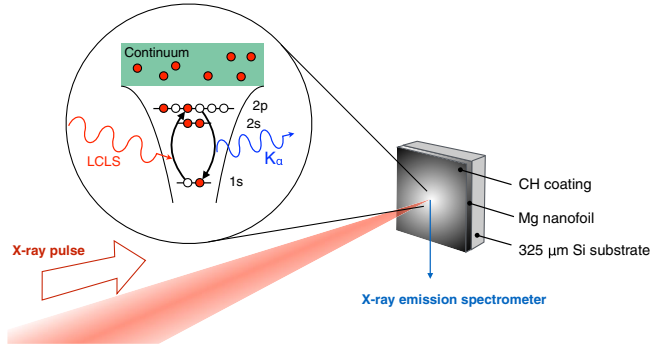


FIG. 1. Experimental setup: A (54 ± 2) -nm-thick Mg foil is irradiated by the focused x-ray pulse. The x-ray wavelength is tuned to the bound-bound resonance in a 7^+ Mg ion, resonantly driving a $1s \rightarrow 2p$ transition creating a core-hole excited state. The excited state can then decay through Auger recombination or K_α emission.

experiment is schematically shown in Fig. 1. We focus a bright 60 fs x-ray pulse onto a 54 nm (± 2 nm) Mg foil on resonance with the $1s \rightarrow 2p$ transition in a 7^+ Mg ion (at 1304 eV). The peak intensity of the x-ray pulse is $\sim 10^{17}$ W cm $^{-2}$, sufficient to heat the sample to temperatures exceeding 100 eV. The central photon energy is chosen below the K edge of all Mg ion charge states, but the slight jitter in the wavelength and the 0.4% FWHM bandwidth (~ 5 eV) of the LCLS pulse enable some pumping of the ground-state K -alpha line via K -shell photoionization. This emission is easily distinguished from the driven resonance, as can be seen in Fig. 2, and acts to increase the energy deposition into, and hence heating efficiency of, the Mg plasma.

The pulse rapidly heats the target, and a combination of L -shell photoionization and electron collisional L -shell ionization burn through the charge states until the 7^+ ion with superconfiguration K^2L^3 is reached (two electrons in the K shell, three in the L shell). At this point, the x-ray pulse resonantly induces a $1s \rightarrow 2p$ transition and produces a core-hole population, as illustrated in Fig. 1. In what follows, we will index the charge state of the Mg ion via the K - and L -shell populations [27,28]. The x-ray bandwidth is sufficiently narrow to pump only a single charge state on resonance. Once created, the core-hole excited state can undergo Auger decay, radiative decay, or further L -shell collisional ionization and recombination. These latter processes, of particular interest to this work, are driven by the heated free-electron population, where a non-negligible proportion of electrons has sufficient kinetic energy to induce an L -shell ionization event. The x-ray pulse is sufficiently bright to excite a sizable fraction of the 7^+ ion population within the focal area and to induce a repeated sequence of excitation and decay [29].

A flat-crystal spectrometer records the time-integrated emission spectrum resulting from radiative decay of core-hole states. Upon radiative decay, each charge state emits at

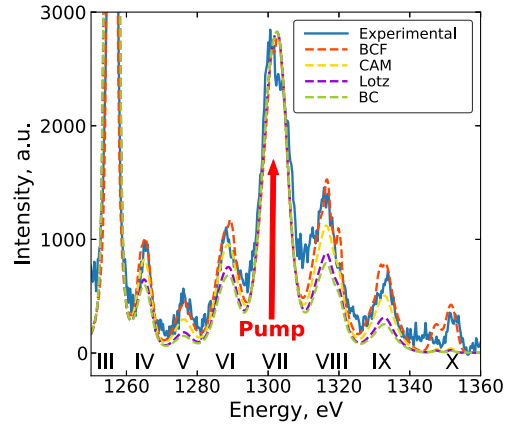


FIG. 2. Experimental and simulated (with the BCF, CAM, Lotz, and BC models) K_α emission spectrum resulting from resonantly driving the $K^2L^3 \rightarrow K^1L^4$ transition centered around 1300 eV. After excitation, the states relax through collisional ionization (up in charge) and three-body recombination (down in charge). The numerals below each emission line denote the charge state of the emitting ion, III thus indicating the cold K_α line.

a characteristic wavelength that allows us to measure the charge-resolved spectrum. Importantly, we note that the measured bound-bound emission intensity is directly proportional to the core-hole ion population only in the optically thin limit. We achieve an optically thin plasma, yet at solid density, by using 54-nm-thick films of Mg, deposited on Si substrates and appropriately coated with a thin CH layer to prevent surface oxidation and sample degradation, as illustrated in Fig. 1. Simulations using the code SCFLY indicate peak optical depths significantly below 0.1 across the Mg emission spectrum for this sample thickness, and the optically thin nature of the plasmas was confirmed experimentally by noting the emission intensity was proportional to the target sample thickness, as discussed in detail by Preston *et al.* [30].

We show in Fig. 2 the experimental and simulated emission spectra, where the numerals below each line denote the charge state of the emitting ion. Disregarding the main K_α line (III) generated by photoionization, the strongest emission is observed from the resonantly pumped line VII. Strong emission can also be observed from off-resonance lines on either side of the resonance. This emission is due to collisional dynamics taking place in the Mg L shell and can be achieved only via a multistep process that starts once the K^1L^4 ion is created via photoexcitation. Before decaying through Auger or radiative recombination back to the ground state, the core-hole ions can undergo collisional ionization ($\rightarrow K^1L^3$) or three-body recombination ($\rightarrow K^1L^5$) and will subsequently decay emitting as a different line. Since the cross section for L -shell photoionization is several orders of magnitude smaller than that for collisional ionization once the system is hot, there is no other efficient way to produce the observed off-resonance lines, and their presence can be

entirely attributed to collisions. Line intensity ratios are therefore a measure of how fast these collisional interactions take place relative to the natural lifetime of a core-hole state. This introduces a time unit against which to clock collisional events: the natural lifetime of core-hole ions. In low- Z elements like Mg, core-hole lifetimes are determined predominantly by Auger decay. The observation in Fig. 2 that multiple collisional processes take place before the core-hole state decays indicates that CI occurs on time scales comparable to Auger lifetimes, of the order of 1–10 fs.

The emission spectrum displayed in Fig. 2 is accompanied by simulations performed with the non-LTE radiative-collisional code SCFLY [17,31,32]. The parameters of the simulation are determined by the measured total pulse energy and the averaged spatial intensity distribution on target via the fluence scan technique [33]. The code self-consistently calculates the time-dependent non-LTE evolution of the system given the interaction with the x-ray FEL pulse, assuming instant thermalization of the free-electron population (the free-electron distribution is assumed to be Maxwellian). We use configuration-averaged Auger lifetimes calculated within the relativistic Dirac-Hartree-Slater approximation [34,35]. Each simulation shown in Fig. 2 uses a different collisional cross section model, namely, those proposed by Clark, Abdallah, and Mann (CAM) [36], Lotz [37], Burgess and Chidichimo (BC) [38], and a new model presented here. Our model uses a functional form similar to the work of Clark and Sampson [39] and the ionization potential depression (IPD) scaling introduced by Fontes, Sampson, and Zhang [40,41] but differs by the fact that it is imposed to be consistent with Lotz and BC in the atomic limit where experimental data are abundant. This new model for the collisional cross section, which we shall refer to as BCF in what follows, is given by the following expression:

$$\begin{aligned} \sigma_{\text{BCF}}(\varepsilon) = & \frac{\pi a_0^2}{(I_i/I_H)^2} \frac{\zeta_i I_i}{R_0^4 \varepsilon} \left\{ \left(c_1 + \frac{c_2 + c_3 l}{n} \right) \log(\varepsilon/I_i) \right. \\ & + R_0 \left(c_4 + \frac{c_5 + c_6 l}{n} \right) \left(1 - \frac{I_i}{\varepsilon} \right) \\ & \left. + R_0^{r_n} \left(c_7 + \frac{c_8 + c_9 l}{n} \right) \left(1 - \frac{I_i}{\varepsilon} \right)^2 \right\}, \quad (1) \end{aligned}$$

where n and l represent the principal and angular momentum quantum numbers, respectively, ε is the incident electron energy, ζ_i is the effective number of electrons in the i th subshell, I_i is the effective ionization threshold, z is the initial charge before ionization, I_H is the Rydberg constant, and a_0 is the Bohr radius. The constants $\{c_1 \dots c_9\} = \{1.0633, 0.6895, -0.4284, 1.6925, -1.7140, 2.2244, -0.5020, 0.5961, -0.1629\}$ are charge- and material-independent fitting constants, and $R_0 = I'/I$ is the ratio between ionization potentials with and without continuum

lowering. The exponent r_n was set by Fontes, Sampson, and Zhang as $\{2.20, 1.90, 1.73, 1.65, 1.60, 1.56, 1.54, 1.52\}$ for $n = \{1-7, \geq 8\}$ [40]. In the atomic limit, $I'_i = I_i$ and $R_0 = 1$, and the model is consistent with BC in the limit of $I_i/\varepsilon \rightarrow 1$. The logarithmic term in Eq. (1) mainly describes the high-energy tail of the cross section, whereas the terms proportional to $(1 - I'_i/\varepsilon)$ and $(1 - I'_i/\varepsilon)^2$ represent behavior in the near-threshold region.

The simulations are highly sensitive to the collisional cross section model. Most notably, the Lotz and BC models severely underestimate all off-resonance peak intensities driven by electron collisional dynamics. Both the Lotz and BC cross sections were originally derived from experimental data in an electron density range of 10^{14} – 5×10^{16} cm $^{-3}$ (later referred to as the “low-density” regime); for details on the experiments and density conditions, we refer to Refs. [42] and Refs. [22,43], respectively. In contrast, the CAM cross section was obtained from fits to theoretical data calculated in the Coulomb-Born-Oppenheimer approximation [44]. The BCF model aims to describe both the aforementioned experimental data in the low-density regime as well as a scaling method to correctly capture the effect of continuum lowering, thereby obtaining a model that is consistent with experimental data both in low- and high-density conditions.

Rate coefficients are obtained by integrating the cross section over the electron distribution, here assumed Maxwellian. L -shell ionization thresholds are reduced by continuum lowering which was determined experimentally in conditions very similar to those of our experiment [28]. Our modeling of this effect is parametrized using the Ecker-Kröll (EK) IPD model [27,45], which reproduces the experimental values to within 10%. Importantly, our observations of collisional rates in Fig. 2 do not depend on our choice of IPD modeling; the IPD matters only insofar as it is needed to predict collisional rates from collisional cross sections. An IPD model which predicts lower levels of continuum lowering would simply require a much larger collisional cross section to reproduce the observed collisional rate. It is by joining the present measurement of collisional rates with previous experimental work on IPD that we are able to infer the form of collisional cross sections in these extreme plasma conditions.

Our SCFLY calculations account for the full non-LTE behavior in the ion populations. However, they indicate that both the ground state and, to a slightly lesser extent, the excited state of the pumped transition are present in electron temperature-density conditions close to LTE. We illustrate this in Fig. 3, where we show at what temperatures and densities the Mg 7 $^+$ ion is present in the non-LTE simulation, taking into account the full temporal evolution and transverse spatial gradients in the target. The ground state of the pumped transition (K^2L^3) is seen to be present in conditions very close to LTE,

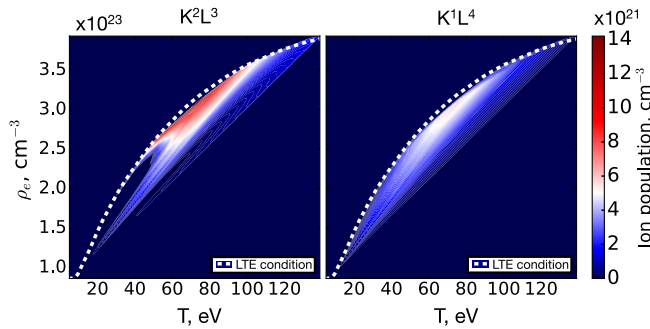


FIG. 3. Simulated evolution of the pumped K^2L^3 (left) and K^1L^4 (right) populations in temperature-density space. Charge state populations are obtained from SCFLY simulations using the BCF model [Eq. (1)] that match the experimental conditions and are binned in a 2D temperature-density histogram across all points in time and space. Both populations peak near the LTE conditions, represented by the white dotted curve.

indicating the ground state is well equilibrated by successive collisions in the dense plasma. The core-excited state (K^1L^4), while clearly not in equilibrium, retains much of this characteristic but is shifted to slightly higher temperatures, as it takes some time to produce via photopumping the ground state, during which the system heats. Since the non-LTE populations closely follow LTE predictions, we note that there is a relatively narrow temporal and spatial window of emission for each charge state configuration. Correspondingly, there is a narrow band of temperatures and densities where each ion population is present. For example, from Fig. 3, we see that the K^1L^4 excited state will emit a photon predominantly at temperatures around 75 eV and at electron densities around $3 \times 10^{23} \text{ cm}^{-3}$. We further note the efficiency of the x-ray pump: over the course of the x-ray pulse, roughly half of the total ground-state population is excited to a core-hole state.

Additional dense-plasma effects that need to be considered alongside continuum lowering are the variations in transition rates with electron density, most notably the Auger and radiative decay rates [46]. Belkhiri and Fontes suggest the Auger rate may be reduced by 2%–3% in solid-density Al plasmas [47], thus slightly increasing core-hole ion lifetimes. This effect is partly compensated for by the radiative decay rates also being decreased, weakening the overall effect on emitted line intensities. We conclude that this effect will have a negligible impact on the measurement here.

After constraining the plasma conditions, accounting for IPD and for possible variations in the Auger rate, our experimental data can be modeled successfully only with the BCF model given in Eq. (1). This model is by definition consistent with other collisional ionization models in the atomic limit, including semiempirical models, yet scales differently from the Lotz and BC models in the dense, strongly coupled regime. The nature of this scaling is important, because collisional ionization processes can no

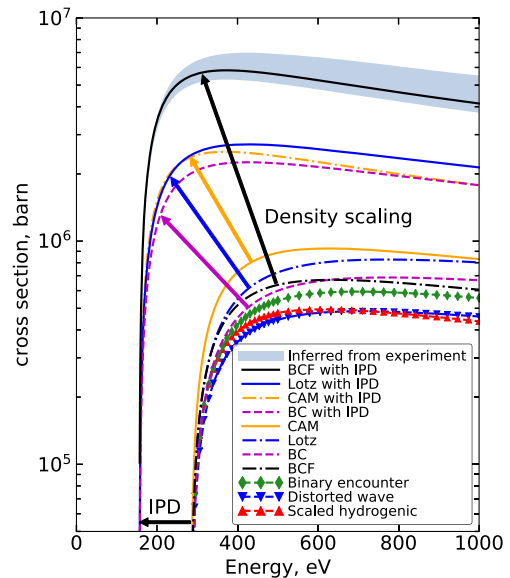


FIG. 4. Collisional ionization cross section for the K^1L^4 (7^+) Mg ion. Theoretical and semiempirical models predict similar cross sections in the atomic limit. Accounting for increasing density via IPD lowers the threshold and raises the cross section; here the BCF model differs significantly from the Lotz and BC models. The range of cross sections consistent with our experimental results shown in Fig. 1 lies within the shaded band.

longer be considered binary events at high densities but become increasingly many-body screened interactions [48]. Such effects are most important near the ionization threshold [49], i.e., for electrons with kinetic energies comparable to the ionization potential, so obtaining the correct scaling of the collisional cross sections with density remains of paramount importance to model collisions in the warm-dense matter regime.

Modeling the plasma evolution with different collisional rate models in SCFLY does not significantly change the conditions under which the $2p \rightarrow 1s$ transition takes place, as the LTE relations remain generally valid. The main difference is that the plasma ionizes at a different pace, and the emission takes place at a different point in time.

The increased collisionality can be attributed to thermal electrons, rather than nonthermal electrons produced via Auger decay or L -shell photoionization, as the thermal collisions are strongly dominant once the conditions of peak emission are reached at temperatures above $\sim 70 \text{ eV}$ [17]. Nonthermal collisions would also tend to affect lower charge states more than higher states, leading to a skew in the emission spectrum for nonresonant lines which is not observed experimentally. We have conducted simulations with the BIGBART code [7,50], which explicitly considers nonthermal electron distributions, and have confirmed that nonthermal electrons affect the CI rates by less than 10% in our experimental conditions.

Because of the need to include density effects in line into the atomic kinetics calculations, the collisional cross

sections used in SCFLY are in parameterized form and scale for core-hole ions as dictated by the shell populations and ionization thresholds. While this may not be the most accurate way to model a core-hole state, we show in Fig. 4 that such cross sections (Lotz, BC, CAM, and BCF models) agree relatively well in the atomic limit with other theoretical results obtained from the Los Alamos Atomic Physics code suite, via scaled hydrogenic [36,44,51], distorted wave [52–55] and binary encounter calculations [56–59]. In Fig. 4, we also show how the parameterized models scale with increasing density. The range of cross sections consistent with our experimental results from Fig. 2 is shown as the shaded region in Fig. 4. We note that, while the IPD is the same for all models, the scaling of the cross sections can be very different within different models, leading to the BCF model predicting a cross section approximately 2.7 times larger than those of the BC or Lotz models. As was already clear from the spectral modeling in Fig. 2, only the BCF model matches with the experimental range.

In summary, we have presented experimental measurements of femtosecond collisional ionization dynamics in solid-density, yet optically thin Mg, showing that collisional ionization and recombination cross sections in the warm-dense matter regime are larger than predicted by several widely used models. A bright, narrow bandwidth x-ray FEL pulse was used to drive a $1s \rightarrow 2p$ resonance in highly ionized Mg ions, and the relaxation of the system was investigated via x-ray emission spectroscopy in a plasma very close to LTE. We have presented a collisional ionization cross section model that is in excellent agreement with the experimental results following detailed collisional-radiative modeling using the non-LTE code SCFLY. We have shown that accounting for the density dependence of collisional cross sections near the threshold is of key importance, over and beyond the aspects of ionization potential depression alone. We note that the observed faster rates of collisional ionization are beneficial for the establishment of LTE conditions on femtosecond time scales in nonequilibrium systems. The higher cross sections at high electron densities can have far-reaching consequences, as transport properties such as the conductivity typically scale with the inverse of the electron-ion collision frequency. Additionally, more efficient collisional dynamics could further limit the time scales before the onset of observable electron damage in nonperiodic nanoscale samples, such as viruses [60] or disordered crystals [61], investigated via coherent diffraction imaging experiments on FELs at ultrahigh x-ray intensities.

We thank C. Spindloe and Scitech Precision Ltd. for manufacturing and characterizing our target samples. Use of the Linac Coherent Light Source (LCLS), SLAC National Accelerator Laboratory, is supported by the U.S. Department of Energy, Office of Science, Office of Basic Energy Sciences under Contract No. DE-AC02-76SF00515.

Q. v. d. B., E. V. F.-T., P. V., and S. M. V. gratefully acknowledge support from the Royal Society. S. M. V. further thanks the United Kingdom Engineering and Physical Sciences Research Council (EPSRC) for support under Grant No. EP/P015794/1. E. V. F.-T. and P. V. further thank No. AWP15-ENR-01/CEA-02 and European Union Horizon 2020 Grant No. 665207. P. H., T. R. P., O. C., and J. S. W. thank the United Kingdom EPSRC for support under Grant No. EP/L000849/1. T. B., J. C., V. H., V. V., and L. J. appreciate financial support from the Czech Science Foundation (Grants No. 17-05167S and No. 17-05076S) and the Czech Ministry of Education (Grants No. LG15013 and No. Z.02.1.01/0.0/0.0/16_013/0001552).

*quincy.vandenberg@physics.ox.ac.uk

†sam.vinko@physics.ox.ac.uk

- [1] O. Peyrusse, *J. Phys. B* **32**, 683 (1999).
- [2] A. Ng, D. Parfeniuk, P. Celliers, L. DaSilva, R. M. More, and Y. T. Lee, *Phys. Rev. Lett.* **57**, 1595 (1986).
- [3] D.-K. Kim and I. Kim, *Phys. Rev. E* **68**, 056410 (2003).
- [4] L. Spitzer and R. Härm, *Phys. Rev.* **89**, 977 (1953).
- [5] G. Miloshevsky and A. Hassanein, *Phys. Rev. E* **92**, 033109 (2015).
- [6] S. B. Hansen *et al.*, *Phys. Plasmas* **21**, 031213 (2014).
- [7] A. G. de la Varga, P. Velarde, F. de Gaufridy, D. Portillo, M. Cotelo, A. Barbas, A. González, and P. Zeitoun, *High Energy Density Phys.* **9**, 542 (2013).
- [8] J. D. Lindl, P. Amendt, R. L. Berger, S. G. Glendinning, S. H. Glenzer, S. W. Haan, R. L. Kauffman, O. L. Landen, and L. J. Suter, *Phys. Plasmas* **11**, 339 (2004).
- [9] F. J. Rogers and C. A. Iglesias, *Science* **263**, 50 (1994).
- [10] R. Neutze, R. Wouts, D. van der Spoel, E. Weckert, and J. Hajdu, *Nature (London)* **406**, 752 (2000).
- [11] E. K. Curwood, H. M. Quiney, and K. A. Nugent, *Phys. Rev. A* **87**, 053407 (2013).
- [12] C. Caleman, M. Bergh, H. A. Scott, J. C. H. Spence, H. N. Chapman, and N. Timneanu, *J. Mod. Opt.* **58**, 1486 (2011).
- [13] S. M. Vinko *et al.*, *Nat. Commun.* **6**, 6397 (2015).
- [14] P. Emma *et al.*, *Nat. Photonics* **4**, 641 (2010).
- [15] S. M. Vinko *et al.*, *Nature (London)* **482**, 59 (2012).
- [16] S. M. Vinko, *J. Plasma Phys.* **81**, 365810501 (2015).
- [17] O. Ciricosta, S. M. Vinko, H. Chung, C. Jackson, R. W. Lee, T. R. Preston, D. S. Rackstraw, and J. S. Wark, *Phys. Plasmas* **23**, 022707 (2016).
- [18] L. J. Kieffer and G. H. Dunn, *Rev. Mod. Phys.* **38**, 1 (1966).
- [19] F. A. Harrison, *Br. J. Appl. Phys.* **17**, 371 (1966).
- [20] B. P. S. O. Martin and K. T. Dolder, *J. Phys. B* **1**, 537 (1968).
- [21] H. J. Kunze, *Phys. Rev. A* **3**, 937 (1971).
- [22] E. Kallne and L. A. Jones, *J. Phys. B* **10**, 3637 (1977).
- [23] W. L. Rowan and J. R. Roberts, *Phys. Rev. A* **19**, 90 (1979).
- [24] D. Crandall, R. Phaneuf, B. Hasselquist, and D. Gregory, *J. Phys. B* **12**, L249 (1979).
- [25] H. R. Griem, *J. Quant. Spectrosc. Radiat. Transfer* **40**, 403 (1988).
- [26] E. K. L. A. Jones and D. Thomson, *J. Phys. B* **10**, 187 (1977).
- [27] O. Ciricosta *et al.*, *Phys. Rev. Lett.* **109**, 065002 (2012).
- [28] O. Ciricosta *et al.*, *Nat. Commun.* **7**, 11713 (2016).

- [29] B. I. Cho *et al.*, *Phys. Rev. Lett.* **109**, 245003 (2012).
- [30] T. R. Preston *et al.*, *Phys. Rev. Lett.* **119**, 085001 (2017).
- [31] H.-K. Chung, M. Chen, W. Morgan, Y. Ralchenko, and R. Lee, *High Energy Density Phys.* **1**, 3 (2005).
- [32] H.-K. Chung, M. Chen, and R. Lee, *High Energy Density Phys.* **3**, 57 (2007).
- [33] J. Chalupský *et al.*, *Opt. Express* **18**, 27836 (2010).
- [34] M. H. Chen, B. Crasemann, and H. Mark, *Phys. Rev. A* **21**, 436 (1980).
- [35] M. H. Chen, *Phys. Rev. A* **31**, 1449 (1985).
- [36] R. E. H. Clark, J. Abdallah, Jr., and J. B. Mann, *Astrophys. J.* **381**, 597 (1991).
- [37] W. Lotz, *Z. Phys.* **216**, 241 (1968).
- [38] A. Burgess and M. C. Chidichimo, *Mon. Not. R. Astron. Soc.* **203**, 1269 (1983).
- [39] R. E. H. Clark and D. H. Sampson, *J. Phys. B* **17**, 3311 (1984).
- [40] C. J. Fontes, D. H. Sampson, and H. L. Zhang, *Phys. Rev. A* **48**, 1975 (1993).
- [41] A. G. de la Varga, doctoral thesis ETSII, UPM, <http://oa.upm.es/32905/>, 2014.
- [42] M. A. Lennon, K. L. Bell, H. B. Gilbody, J. G. Hughes, A. E. Kingston, M. J. Murray, and F. J. Smith, *J. Phys. Chem. Ref. Data* **17**, 1285 (1988).
- [43] D. Crandall, R. Phaeuf, and D. Gregory, Report No. ORNL/TM-7020, Oak Ridge National Laboratory, 1979.
- [44] L. B. Golden and D. H. Sampson, *J. Phys. B* **10**, 2229 (1977).
- [45] T. R. Preston, S. M. Vinko, O. Ciricosta, H.-K. Chung, R. W. Lee, and J. S. Wark, *High Energy Density Phys.* **9**, 258 (2013).
- [46] M. Belkhir and M. Poirier, *Phys. Rev. A* **90**, 062712 (2014).
- [47] M. Belkhir and C. J. Fontes, *J. Phys. B* **49**, 175002 (2016).
- [48] T. Bornath, M. Schlages, F. Morales, and R. Prenzel, *J. Quant. Spectrosc. Radiat. Transfer* **58**, 501 (1997).
- [49] M. C. Zammit, D. V. Fursa, and I. Bray, *Phys. Rev. A* **82**, 052705 (2010).
- [50] A. G. de la Varga, P. Velarde, M. Cotel, F. de Gaufridy, and P. Zeitoun, *High Energy Density Phys.* **7**, 163 (2011).
- [51] R. M. More, *J. Quant. Spectrosc. Radiat. Transfer* **27**, 345 (1982).
- [52] G. Csanak, H. S. Taylor, and R. Yaris, *Phys. Rev. A* **3**, 1322 (1971).
- [53] S. M. Younger, *Phys. Rev. A* **22**, 1425 (1980).
- [54] J. B. Mann, *At. Data Nucl. Data Tables* **29**, 407 (1983).
- [55] D. H. Sampson, H. L. Zhang, and C. J. Fontes, *Phys. Rep.* **477**, 111 (2009).
- [56] J. Thomson, *Philos. Mag. Ser.* **23**, 449 (1912).
- [57] R. C. Stabler, *Phys. Rev.* **133**, A1268 (1964).
- [58] M. Gryziński, *Phys. Rev.* **138**, A336 (1965).
- [59] A. Burgess and I. C. Percival, *Adv. At. Mol. Phys.* **4**, 109 (1968).
- [60] T. Ekeberg *et al.*, *Phys. Rev. Lett.* **114**, 098102 (2015).
- [61] K. Ayyer *et al.*, *Nature (London)* **530**, 202 (2016).